

Article

Effect of the Support on Rhenium Carbide in the Hydrodeoxygenation of Guaiacol as Lignin-Derived Model Compound

Elodie Blanco ^{1,2,3,*} , Ana Belén Dongil ^{4,*} , Isaac Tyrone Ghampson ⁵ and Néstor Escalona ^{2,3,6,7}

- ¹ Departamento de Ingeniería y Gestión de la Construcción, Pontificia Universidad Católica de Chile, Santiago 7820436, Chile
 - ² Departamento de Ingeniería Química y Bioprocesos, Pontificia Universidad Católica de Chile, Santiago 7820436, Chile
 - ³ ANID (Agencia Nacional de Investigación y Desarrollo de Chile)—Millennium Science Initiative Program- Millennium Nuclei on Catalytic Process towards Sustainable Chemistry (CSC), Santiago 7820436, Chile
 - ⁴ Instituto de Catálisis y Petroleoquímica, CSIC (Consejo Superior de Investigaciones Científicas), Cantoblanco, 28049 Madrid, Spain
 - ⁵ Department of Applied Chemistry for Environment, Graduate School of Urban Environmental Sciences, Tokyo Metropolitan University, 1-1 Minami-Osawa, Hachioji, Tokyo 192-0397, Japan
 - ⁶ Departamento de Química Física, Facultad de Química y de Farmacia, Pontificia Universidad Católica de Chile, Santiago 7820436, Chile
 - ⁷ Centro de Investigación en Nanotecnología y Materiales CIEN-UC, Pontificia Universidad Católica de Chile, Santiago 7820436, Chile
- * Correspondence: elblanco@uc.cl (E.B.); a.dongil@csic.es (A.B.D.)



Citation: Blanco, E.; Dongil, A.B.; Ghampson, I.T.; Escalona, N. Effect of the Support on Rhenium Carbide in the Hydrodeoxygenation of Guaiacol as Lignin-Derived Model Compound. *Catalysts* **2022**, *12*, 1229. <https://doi.org/10.3390/catal12101229>

Academic Editors: Maria Jaworska and Piotr Lodowski

Received: 11 September 2022

Accepted: 10 October 2022

Published: 13 October 2022

Publisher's Note: MDPI stays neutral with regard to jurisdictional claims in published maps and institutional affiliations.



Copyright: © 2022 by the authors. Licensee MDPI, Basel, Switzerland. This article is an open access article distributed under the terms and conditions of the Creative Commons Attribution (CC BY) license (<https://creativecommons.org/licenses/by/4.0/>).

Abstract: The effect of support on the formation of rhenium carbide in the hydrodeoxygenation (HDO) of guaiacol as a lignin-derived compound was evaluated. Catalysts were prepared by incipient wetness impregnation, carburized at 650 °C under a mixture 25/75 of ethylene/hydrogen, and characterized by XRD, N₂-physisorption, TPR, TPD of NH₃ or isopropylamine (IPA), and XPS. The results have demonstrated that the support choice affects the carburization of rhenium. Indeed, over non-acidic support (e.g., SiO₂), limited carburization of the metal was observed, while over ZrO₂ and Al₂O₃, carburization of rhenium occurred, and different carbidic species were obtained depending on the surface and chemical identity of the support. The rhenium carbide species obtained over ZrO₂ was the most active and selective toward benzene (22% at 98% of conversion).

Keywords: HDO; rhenium carbides; acidity

1. Introduction

Increasing concerns about climate change and fossil fuel depletion have intensified the development of renewable alternatives to progressively replace current energy resources in the last few decades. Biomass is recognized as the only raw material that can replace both fuel and chemical production. Biomass is 100% carbon-neutral since it absorbs CO₂ for its growth. It can be transformed by pyrolysis and hydrogenolysis into platform molecules that can be further upgraded into chemical commodities with high added value such as plastics, resin, and chemicals for the pharmaceutical industry. Pyrolysis of biomass produces bio-oil, which is composed of several oxygenated-aromatic monomers [1] and possesses poor calorific capacity, high viscosity, and poor stability over time due to high functionalization [2]. Thus, the oxygen content must be decreased in order to valorize bio-oil. Hydrodeoxygenation (HDO) is a widely used process in that regard [3,4].

Hydrodeoxygenation studies typically involve the use of model compounds such as guaiacol and phenol. Many catalysts have been evaluated, with early studies focusing

on metal sulfides that favor the formation of aromatics such as benzene and toluene xylene (BTX) [5]. However, metal sulfides require the presence of a sulfiding agent in the feed to prevent phase transformation, leading to interest in non-sulfide catalysts. In that regard, noble metal catalysts have generally been reported as the most effective with regards to producing fully hydrogenated compounds [6,7]. Non-noble metallic catalysts, principally Ni, have also been shown to produce high yields of fully hydrogenated compounds, although they are not as stable as noble metal catalysts [8–10]. Other active phases have been investigated, such as oxides [11–13], nitrides [14,15], phosphides [16–18], and carbides [19–21]. In particular, carbides have recently garnered a lot of attention, with Mo_2C being shown to be highly active for several reactions [22–25]. Additionally, the catalytic behavior of Mo_2C can be easily tuned by adjusting the oxygen/carbon content on the metal. In previous work on the HDO of guaiacol over different metal carbides, rhenium carbide (ReC) was shown to be more active than Mo_2C and more selective toward BTX [26]. Subsequent studies led to the optimization of carburization conditions to prepare the carbides using activated carbon as a support [27,28].

Carbon-based materials are often chosen as supports for HDO reactions (especially when carbides are used as the active phase). Using metal oxide supports with different acidic properties, such as ZrO_2 or Al_2O_3 , could expand the versatility of the carbides either through direct participation of the supports in the reaction or through modification of the electronic character of the carbidic phase. This is true for other active phases such as metal sulfides [29], metal oxides [13], and noble metals [30], among others. In those studies, it was shown that CoMoS supported on ZrO_2 led to an efficient conversion of guaiacol into deoxygenated hydrocarbons with totally different selectivities compared to CoMoS supported on Al_2O_3 [29]. A similar trend was observed in the HDO of cresol over a MoO_3 supported on ZrO_2 , where the support stabilized partially reduced, coordinatively unsaturated (CU) sites, leading to high yields of toluene [13]. Finally, in the HDO of phenol over Pd catalysts, it was reported that the use of an oxophilic support such as ZrO_2 favored selectivity towards benzene [30]. It would be interesting to determine if those reported findings manifest when metal carbides are used as the active phase. Indeed, in the case of Mo_2C supported on Al_2O_3 or ZrO_2 for a methanol steam reforming reaction, the methanation reaction was suppressed due to the ability of ZrO_2 to retain methoxy groups while resisting the formation of hydroxyl groups on its surface [31]. On the other hand, in the case of dry reforming, it was reported that by dispersing Mo_2C on Al_2O_3 , novel active acidic sites were produced [32]. Nevertheless, according to our knowledge, in the case of HDO, carbides supported over non-carbon materials have received very little attention.

The present work aims to evaluate the catalytic properties of rhenium carbide supported over non-carbon-based materials. Three supports were considered, namely SiO_2 , Al_2O_3 , and ZrO_2 .

2. Results and Discussion

2.1. Catalysts Characterization

The textural properties obtained from N_2 -sorption isotherms (Figure 1) are summarized in Table 1. Figure 1 shows that all of the supports presented a type IV isotherm typical of mesoporous materials, although the hysteresis loops were different. A type H2 hysteresis was obtained in the case of Al_2O_3 and ZrO_2 , corresponding to the existence of bottle-neck shape pores, while a type H1 hysteresis was obtained for SiO_2 , corresponding to the presence of cylindrical shape pores. The pore size distribution obtained from the desorption branch of the isotherm using the BJH model indicates that ZrO_2 possessed the smallest pore size (ca. 3 nm), followed by Al_2O_3 (ca. 7.5 nm) and then SiO_2 (12.5 nm). Importantly, ZrO_2 presented a narrow pore size distribution, SiO_2 showed a broad pore size distribution, and Al_2O_3 revealed a bimodal pore size distribution. Thus, the supports used presented distinct textural properties.

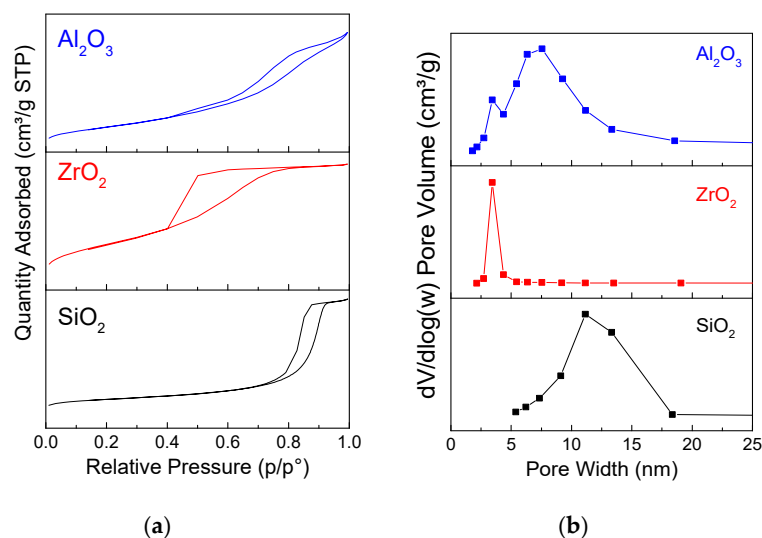


Figure 1. N₂ adsorption-desorption isotherms (a) and pore size distribution (b) of the bare supports.

Table 1. Textural properties for the supports and the resulting catalysts.

		S _{BET} (m ² g ⁻¹)	Pore Volume (cm ³ g ⁻¹)		
			V _μ	V _{meso}	V _T
Al ₂ O ₃	Support	327	0	0.43	0.43
	Catalyst	206	0	0.41	0.41
SiO ₂	Support	458	0.03	1.63	1.66
	Catalyst	278	0	1.01	1.01
ZrO ₂	Support	112	0	0.09	0.09
	Catalyst	80	0	0.09	0.09

Table 1 shows that surface areas of SiO₂ and Al₂O₃ decreased after the impregnation/carburization of Re. However, the decrease was more pronounced than would be expected for a 10 wt% metal loading, suggesting some degree of pore blockage by Re species. The surface area of ZrO₂ also decreased upon Re introduction and the subsequent thermal treatments, although the decrease was less drastic compared to the other catalysts and may be largely due to the presence of Re in the catalyst. This suggests the absence or minimal occurrence of pore blockage and the uniform distribution of Re species in the porous structure of the ZrO₂ support.

Figure 2 shows XRD patterns of the catalysts. In the case of ReC/Al₂O₃, peaks associated with the support can be observed (γ -Al₂O₃, 00-001-1303), along with weak features around 20° and 30° 2 θ , possibly due to rhenium aluminate (00-020-0052). For ReC/ZrO₂, peaks corresponding to the tetragonal phase of ZrO₂ was identified (00-079-1769), in addition to a diffraction plane related to Re⁰ (01-087-0599). Notably, there is a shift to higher angle for the Re⁰ feature (Figure 2b), which has previously been ascribed to incorporating carbon into the matrix during carburization and gives evidence for carbide/oxycarbide formation [28]. In the case of ReC/SiO₂, peaks indexed as Re⁰ phase can be observed. The results suggest that the nature and dispersion of the Re species is influenced by the type of support, with ZrO₂ favoring the formation of small carbide/oxycarbide particles, SiO₂ favoring the formation of large metallic particles, and Al₂O₃ interacting strongly with Re species.

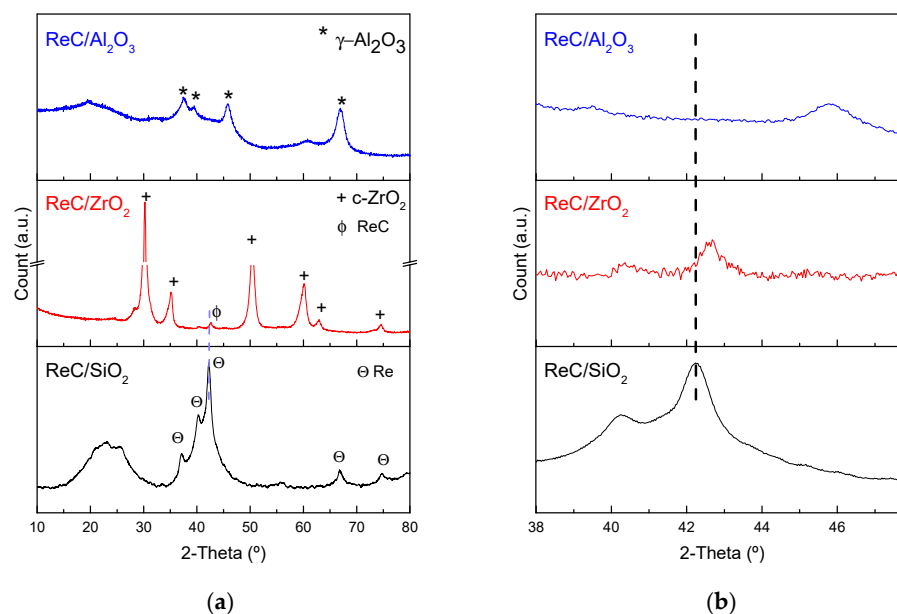


Figure 2. Diffractograms obtained for the catalysts (a), zoom in the region from 38° to 48° (b).

Figure 3 and Table 2 show the surface composition of the catalysts determined by XPS. As noted previously, the passivated catalysts were re-reduced at 350 °C for 30 min under H₂ to mimic the conditions during reaction.

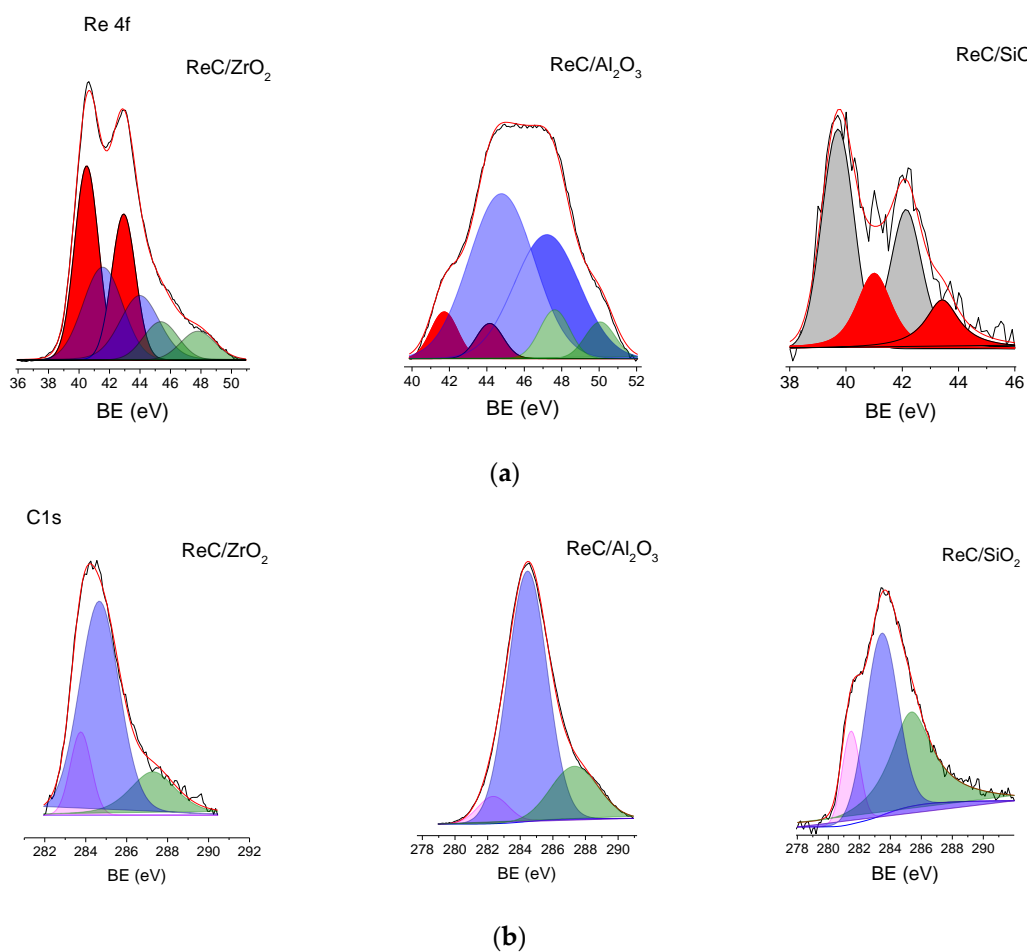


Figure 3. XPS deconvolution of the Re 4f (a) and C 1s (b) component.

Table 2. XPS data obtained for the catalysts after in situ re-reduction at 350 °C.

Catalyst	BE, eV (%)								
	Re 4f _{7/2}					C 1s			
	Re ⁰	Re ^{δ+}	Re ²⁺	Re ⁶⁺	Re ⁷⁺	Carbide	C=C	C-C	C=O
ReC/SiO ₂	40.2 (68)		41.5 (38)			282.6 (12)	284.6 (43)	286.4 (44)	
ReC/Al ₂ O ₃			41.7 (9)	44.8 (80)	47.6 (11)	282.3 (6)	284.4 (75)		287.3 (19)
ReC/ZrO ₂		40.5 (48)	41.6 (38)		45.4 (14)	283.7 (13)	284.6 (68)		287.3 (19)

Table 2 shows that the Re 4f band can be fitted to two components for ReC/SiO₂ and to three components for ReC/Al₂O₃ and ReC/ZrO₂. The binding energy (BE) of the different Re species detected were at 40.2, 40.5, 41.6, 44.8, 45.4 and 47.6 ± 0.1 eV. The BE at 40.2 eV can typically be assigned to Re⁰ species [33], the one at 40.5 eV was previously ascribed to partially carburized Re (Re^{δ+}) [27], the component at 41.6 eV can be ascribed to Re²⁺ species [34], and the BE at 44.8 eV can be attributed to Re⁶⁺ [34]. The attribution of the remaining species is more complicated as BE of Re is known to shift significantly due to oxygen vacancies [34]. Indeed, the bands at 45.4 and 47.6 eV can both be related to Re⁷⁺, although the former has been assigned to Re⁷⁺ in ReO₄⁻ while the latter has been attributed to Re⁷⁺ in Re₂O₇ [33].

The results show clear differences in the nature of the Re species on the surface of the catalysts. The predominant species detected at the surface of ReC/SiO₂ was Re⁰, while the major species on the surface of ReC/ZrO₂ was the partially carburized Re, consistent with XRD results. This suggests that the surface and bulk composition of the ReC/SiO₂ and ReC/ZrO₂ catalysts were similar. The main species present on ReC/Al₂O₃ was Re⁶⁺, followed by Re²⁺. Although Re²⁺ and Re⁶⁺ have been assigned in the literature to ReO and ReO₃ species, respectively, they could also be associated with Re₂C and ReO_xC_y phases, and hence the presence of carbidic phase on ReC/Al₂O₃ cannot be ruled out.

Figure 3 also shows that the C 1s band can be fitted into three components. The component at 282–283.7 eV can be assigned to carbidic carbon [35], the components at 284.0–284.6 eV and 285.8 eV can be attributed to sp² (C=C) and sp³ (C-C) carbon, respectively, and finally the component at 287.3 eV can be ascribed to C=O species [36]. The formation of aromatic carbon during carburization is well documented and is as expected [35], and the formation of a carbide phase in the three catalysts can be confirmed. Nevertheless, the BE of the carbidic band appears quite shifted in the case of the ReC/ZrO₂ support, which may have been induced by the support. It is known that Zr is the most electropositive of all of the support cations, indicating that it has the highest ability to withdraw electrons from the dispersed species. The result is thus consistent with an electronic modification of the carbide phase in the case of ReC/ZrO₂.

Figure 4 displays the TPR profiles of the catalysts. The results consist of the evolution of the TCD signals and the mass fragments corresponding to CH₄ (*m/z* = 15), CO (*m/z* = 28), and CO₂ (*m/z* = 44) formed during the reduction. The TCD signals correspond to H₂ consumed, although it is difficult to obtain clear information on the reduction behavior of carbonaceous species from this result. Here, it is important to remember that the samples are passivated species. Nevertheless, some observations can be made. The TCD signal of the ReC/SiO₂ catalyst displays two features at around 150 and 380 °C and a sharp drop at around 600 °C. The feature at 150 °C can be assigned to the reduction of the passivation layer, and the feature at 380 °C can be attributed to the reduction of ReO_x species [11,37]. The sharp drop coincided with the formation of CO and could be associated with the reduction of some oxycarbide species. The TCD signals for ReC/ZrO₂ and ReC/Al₂O₃ also show the same two lower-temperature features observed for the ReC/SiO₂ (150 and 350 °C), along with an additional feature around 500 °C. The higher-temperature feature could be due to the existence of particles that interacted more strongly with the support.

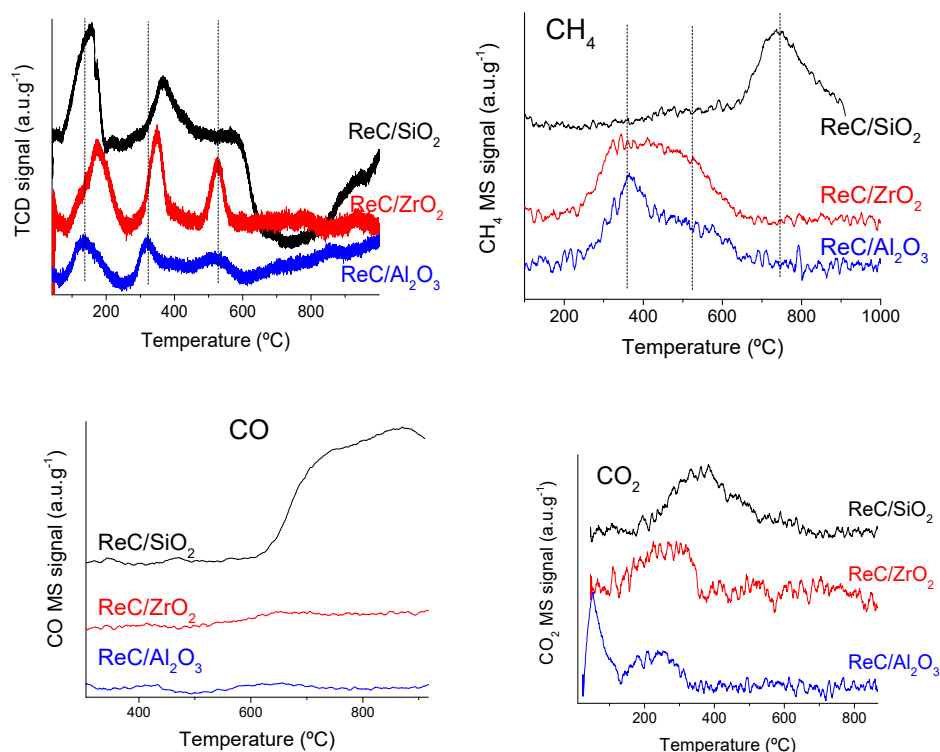


Figure 4. Evolution of the TCD signal and MS fragments of CH_4 , CO , and CO_2 formed during TPR.

The CH_4 traces give additional insights into the species present on the catalysts. In the case of ReC supported over Al_2O_3 and ZrO_2 , the last feature at around 500°C is accompanied by CH_4 formation. According to the literature, CH_4 results from gasification reaction and can be associated with different carbon species depending on the temperature [28,38,39]. For this reason, the CH_4 traces were deconvoluted and the results are presented in Figure 5. For the $\text{ReC}/\text{Al}_2\text{O}_3$ and ReC/ZrO_2 catalysts, three components could be distinguished: 376 , 475 , and 552°C for $\text{ReC}/\text{Al}_2\text{O}_3$; 327 , 412 , and 520°C for ReC/ZrO_2 . The first two peaks correspond to carbidic species, whereas the latter is related to pyrolytic carbon [28,38,39]. Thus, two different carbidic phases were detected on the catalysts, although the lower temperatures obtained for ReC/ZrO_2 suggest that the particles interacted less strongly with the ZrO_2 support than with the Al_2O_3 support.

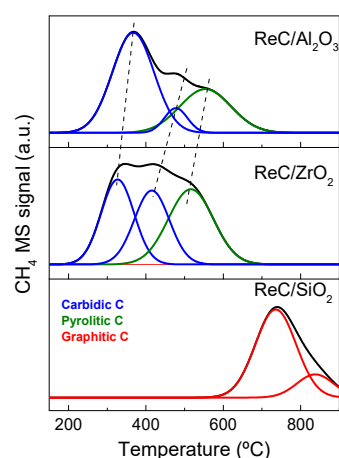


Figure 5. Deconvolution of the CH_4 MS signal for each catalyst.

Finally, the formation of CO_2 could also be appreciated for the three samples with a wide band centered around 400°C in the case of SiO_2 , 300°C for Al_2O_3 and in the case of

ZrO₂, the band is centered at around 250 °C and present a second band at 100 °C. Those band could be associated to the decomposition of some oxygenated carbon species such as carboxylic or lactonic groups [40] or eventually to the reduction of some oxycarbides species [28].

Figure 6 shows NH₃-TPD profiles of the supports and the corresponding catalysts. The results give information on the acidic properties of the catalysts. The desorption profiles for the SiO₂ support and the ReC/SiO₂ catalysts were featureless, indicating the absence of acidic sites. The profiles for the other supports show broad peaks from 100 to 300 °C, indicating the presence of weak and medium acid sites. [41] After the impregnation and carburization steps, the TPD profile shows that NH₃ desorbed between 100 and 200 °C, suggesting that medium acid sites were eliminated likely due to deposition of Re species.

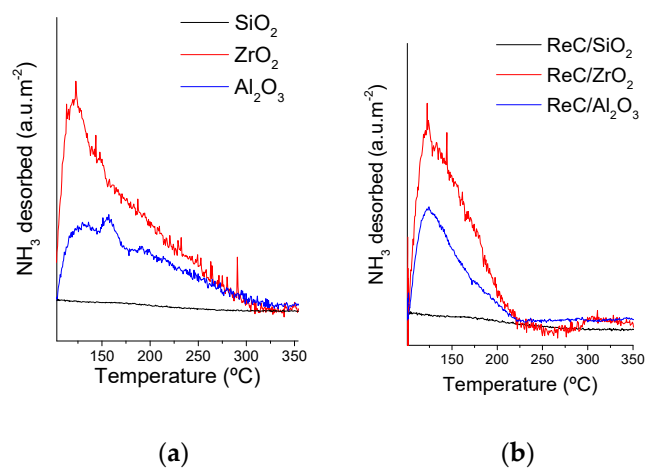


Figure 6. NH₃-TPD profile of the supports alone (a) and the resulting catalysts (b).

Temperature programmed decomposition of isopropylamine (TPD-IPA) was carried out to assess the Brønsted acidity of the supports and the catalyst. It is well-established that IPA decomposes into NH₃ and propene over Brønsted acid sites (BAS) through the Hoffmann elimination reaction [42]. Thus, the MS signal of propene ($m/z = 41$) can be used for comparison of the Brønsted acidity and is presented in Figure 7.

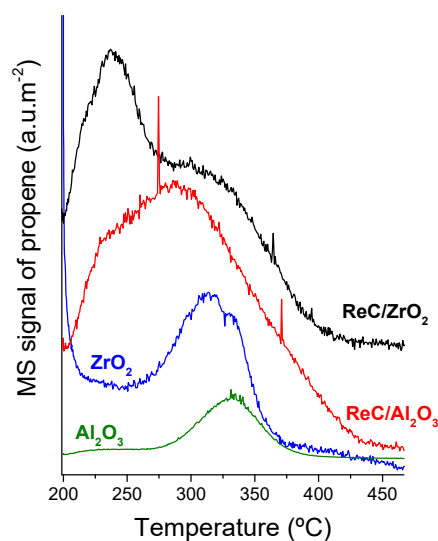


Figure 7. TPD-IPA profile of the supports alone and the resulting catalysts.

It can be observed that in the case of the bare supports, propene is formed at around 320 °C for ZrO₂ and 334 °C for Al₂O₃. The lower temperature observed in the case of

ZrO₂ compared to Al₂O₃ indicates that the BAS on ZrO₂ are stronger than on Al₂O₃. After impregnation and carburization of Re, two features of propene are observed at 238 °C and 312 °C in the case of ZrO₂ and at 239 °C and 291 °C for Al₂O₃. The lower temperature feature is related to strong BAS, whereas the higher temperature feature is due to weak BAS. Interestingly, the addition of the metal increased the amount of BAS on both samples and introduce new acid sites. Additionally, it can be observed that the weaker BAS are more prominent over ReC/Al₂O₃, while the stronger BAS are more prominent on ReC/ZrO₂.

In summary, catalysts characterization results provide clear evidence of support's influence on the nature and dispersion of the active phase obtained after carburization. Over SiO₂, the results suggest that Re⁰ was mainly obtained and carburization was minor. Over ZrO₂, it appears that Re_xC was obtained together with Re₂C. Finally, over Al₂O₃, the data suggest that Re₂C and ReC_xO_y/ReO_x may have been formed. The origin of these differences could reside in the acidity of the support. The desorption profiles of NH₃ indicate that SiO₂ has negligible acidity while Al₂O₃ and ZrO₂ have acid sites of comparable strength. The TPD-IPA results indicate that ZrO₂ presented stronger BAS than Al₂O₃, which may have played a role in the formation of ReC with a higher amount of strong BAS.

2.2. Catalytic Properties

The catalysts and the bare supports were evaluated for guaiacol HDO. Table 3 summarizes the initial rate of conversion (r^0) together with the CO uptakes. Negligible guaiacol conversion was obtained over the SiO₂ support, while appreciable conversions were observed over the ZrO₂ and Al₂O₃ supports. The initial rates over the ZrO₂ support ($9.5 \times 10^{-6} \text{ mol g}^{-1} \text{ s}^{-1}$) was about two times higher than on the Al₂O₃ support ($4.8 \times 10^{-6} \text{ mol g}^{-1} \text{ s}^{-1}$).

Table 3. CO uptake and initial rate of guaiacol conversion obtained at 350 °C.

	SiO ₂	ReC/SiO ₂	ZrO ₂	ReC/ZrO ₂	Al ₂ O ₃	ReC/Al ₂ O ₃
CO uptake ($\mu\text{mol g}^{-1}$)	-	5	-	35	-	28
r^0 ($10^{-6} \text{ mol g}^{-1} \text{ s}^{-1}$)	0	1.5	9.5	14.2	4.8	9.9
TOF (s^{-1})	-	0.30	-	0.41	-	0.35

Table 3 shows that the initial rates over the catalysts decreased in the order, ReC/ZrO₂ > ReC/Al₂O₃ > ReC/SiO₂. The turnover frequency (TOF), reported based on sites counted by CO chemisorption, were different, suggesting that the conversion of guaiacol at the initial stage of the reaction was catalyzed by different active sites. Such differences could be expected as the supports are not inert (except SiO₂), for instance ZrO₂ could account for near 2/3 of initial rate than ReC/ZrO₂ while Al₂O₃ could account for nearly half of the activity of the ReC/Al₂O₃. Interestingly, in the case of ReC/SiO₂, a weak CO uptake was measured despite that Re⁰ was identified as the active phase. One explanation for this could be the presence of graphitic carbon formed during the carburization that might block the access of active site [43–45].

Figure 8 shows a comparison of the product selectivity for the bare supports (Figure 8a) and the catalysts (Figure 8b) at similar conversions. The label "Other" includes methylated compounds such as veratrole, methylated guaiacol, etc.

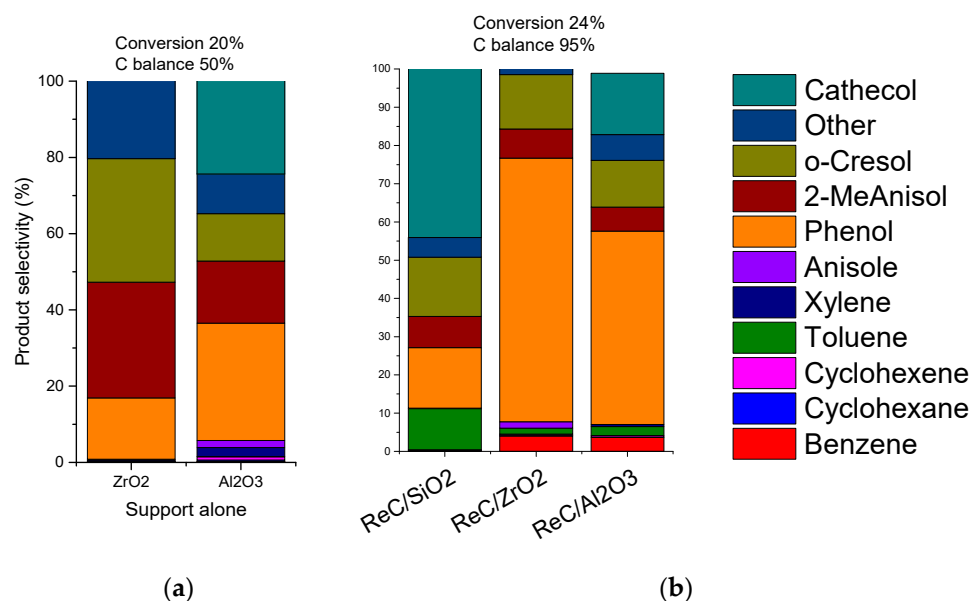


Figure 8. Comparison of the product selectivities obtained at 20–24% of guaiacol conversion and the respective carbon balances over the bare supports (a) and the catalysts (b). Reaction conditions: 200 mg catalyst, 350 °C, 5.0 MPa H₂.

Figure 8 shows that a poor carbon balance was obtained over the bare supports, suggesting strong adsorption of guaiacol on the acid sites of the support or rapid formation of coke. The main products formed over ZrO₂ were cresol, methylanisole, methylated and methoxy compounds, and phenol. These are generally consistent with reported results in the literature, although cyclohexanone was also reported [46]. These products were also observed over the bare Al₂O₃ support. However, catechol was also produced in significant amounts, in addition to anisole, xylene, cyclohexene, which were formed in trace amounts. The results are consistent with those reported in the literature [47,48]. Thus, the results indicate the possible involvement of acid sites on the support in the reaction, although it is not clear whether those sites became inaccessible after the impregnation and carburization of Re species.

The product selectivities over the catalysts show important differences. In the case of ReC/SiO₂, the main product obtained was catechol (44%), followed by cresol and phenol (both 15%), toluene (10%), and then methylanisole (8%). The products observed and the selectivities obtained suggest that demethylation and methyl transfer reactions, along with dehydroxylation, occurred significantly. It was previously shown that Re⁰ was the main surface species present on the ReC/SiO₂ catalyst, indicating that metallic Re species are mainly responsible for the reaction. However, the possible participation of Re²⁺ species cannot be disregarded. Direct comparison of these results to previously published of guaiacol HDO over Re/SiO₂ is difficult due to the differences in the reaction temperature (300 vs. 350 °C) and the likely existence of carbidic Re species in the present work [33,49].

For the ReC/ZrO₂ and ReC/Al₂O₃ catalysts, there were some similarities in product selectivities. Both catalysts were most selective towards phenol, the catalyst ReC/ZrO₂ (68%) being more selective than ReC/Al₂O₃ (50%). In addition, the selectivities to benzene, toluene, 2-methyl-anisole, and o-cresol were similar over the catalysts. The similarities are in line with TPR and in a lesser extent, to XPS results which showed some degree of similarities in the surface species on the catalysts. However, there were some differences, the most notable being the selectivity to catechol over ReC/Al₂O₃ and the lack there of over ReC/ZrO₂. This difference may have arisen from the direct involvement of acid sites associated with the supports influencing the reaction pathway. It was previously observed (Figure 8a) that while the bare Al₂O₃ support was selective to catechol, the bare ZrO₂ support was not. Furthermore, the higher selectivity to phenol and the absence of

catechol over the ReC/ZrO₂ catalyst suggests that this catalyst possessed sites that allowed bypassing of catechol. It is suggested that the existence of the Re_xC phase, as indicated by XPS, played an important role in the direct formation of phenol.

Figure 9 shows the evolution of the products yield and guaiacol conversion. Due to the low conversion, it is difficult to deduce the sequence of products formation from the results for the ReC/SiO₂ catalyst. However, it is clear that catechol was formed initially and remained a dominant product during the course of the reaction. This suggests that subsequent conversion of secondary products was minimal (Figure 10). In the case of ReC/ZrO₂ and ReC/Al₂O₃, the yield profiles of phenol and o-cresol are consistent with those of intermediate products. However, it was not clear from the data if they were primary products due to the appreciable guaiacol conversion even at the onset of reaction. What is clear is that catechol was also formed over ReC/Al₂O₃, and thus it is likely that a fraction of the phenol produced originated from dehydroxylation of catechol.

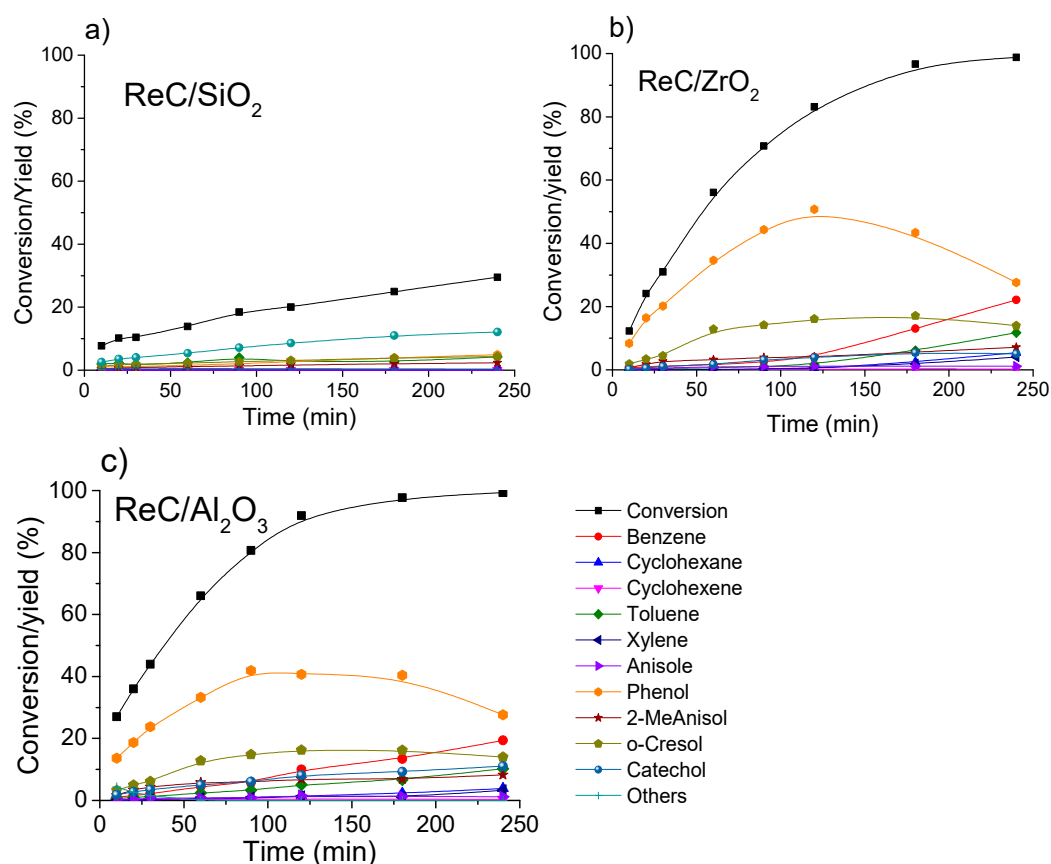


Figure 9. Evolution of guaiacol conversion and the products yield for the different catalyst (a) ReC/SiO₂ (b) ReC/ZrO₂ and (c) ReC/Al₂O₃. Reaction conditions: 200 mg catalyst, 350 °C, 5.0 MPa H₂.

Another important observation is the yield of benzene: it can be observed that benzene was subsequently formed, which is in general agreement with other previous reports concerning carbides [27]. However, there was one important difference between this result and the previous one. In the previous study over ReC/AC, conversion of phenol to benzene only began once guaiacol had been completely converted, which was attributed to the competitive adsorption of phenol with guaiacol [27]. In the present case, conversion of phenol to benzene began when guaiacol conversion reach around 80%. It is reasonable that acid sites present over the ZrO₂ and Al₂O₃ supports may have aided in the adsorption of phenol, facilitating its conversion to benzene even at lower guaiacol conversion. Also, the yield of toluene, likely formed from hydroxylation of o-cresol, increased with increasing

reaction time. It is important to remark that the significant yields of benzene and toluene (aromatic hydrocarbons) and the substantially low yields of cyclohexane and cyclohexene (fully hydrogenated compounds) is indicative of the contribution of the supports in minimizing hydrogenation, particularly when compared to the results of ReC/AC [27].

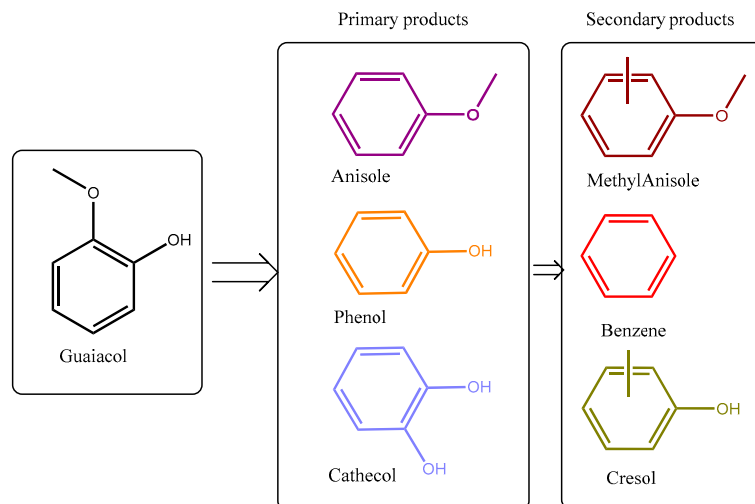


Figure 10. Main product obtained from guaiacol HDO over Re-based catalysts.

Finally, the evolution of the products that contain 0,1, or 2 oxygen with time are presented in Figure 11 to compare more specifically how efficient are the catalysts in the HDO compared to other reactions. In this figure, others represent methylated products obtained over acid sites. Figure shows that a similar trend is obtained on both supports with some slight differences such as the formation of a lower amount of others over ZrO_2 than Al_2O_3 at high conversion on the benefit of completely deoxygenated products (ca. 0-oxygen). This figure demonstrated that the carbide obtained over ZrO_2 is more selective toward HDO reactions than Al_2O_3 .

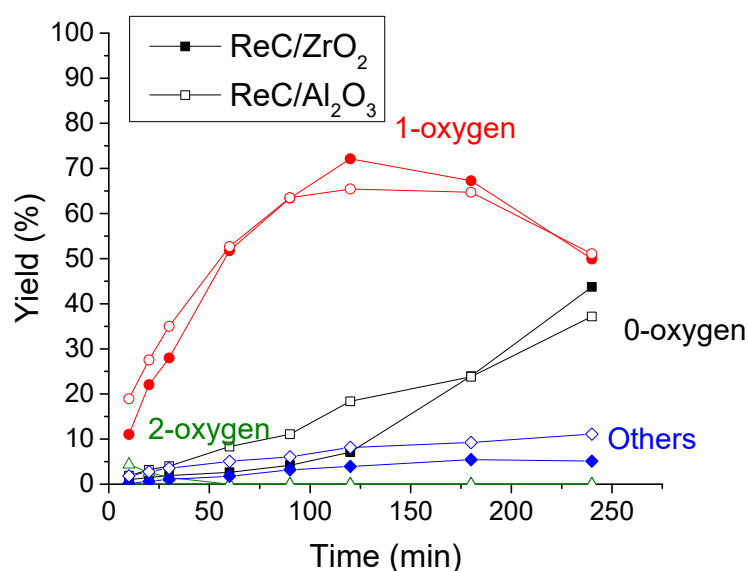


Figure 11. Evolution with time of the reactions products groups by their amount of oxygen.

3. Materials and Methods

3.1. Materials

The chemicals used in this study were $ZrOCl_2$ (99%, Merck, Darmstadt, Germany), NH_4ReO_4 (99%, Sigma-Aldrich, Darmstadt, Germany), aqueous NH_3 (25%, Loba Chemi

PVT, Mumbai, India), Al₂O₃ (SPH 501 A, Rhodia, France), SiO₂ (Grace, USA), dodecane, hexadecane, guaiacol (all reagent grade, Merck, Darmstadt, Germany). The gases used were purchased from Indura (Chile).

3.2. ZrO₂ Synthesis

ZrO₂ was prepared by a precipitation method, according to a procedure reported by Znaiguia et al. [50] Typically, ZrOCl₂ (0.4 M) was added dropwise to an aqueous solution of NH₃ (25%) under stirring and the pH was maintained at 9. The mixture was left for 2 h, filtered, and then washed with deionized water until a neutral solution was obtained. The solid was finally calcined under air at 450 °C for 1 h.

3.3. Catalyst Preparation

Catalysts were prepared by incipient wetness impregnation (IWI) of an aqueous solution of NH₄ReO₄ over the supports (nominal content of Re was fixed at 10 wt%). The supports were previously ground, sieved ($\leq 150 \mu\text{m}$), and dried at 110 °C for 2 h. After impregnation, the mixture was left for 6 h at room temperature for maturation and dried for 15 h at 80 °C. Then, the catalysts were carburized at 650 °C for 1.5 h under a flow (100 mL min⁻¹) of 75% H₂/25% C₂H₄. These conditions were chosen according to the previous studies [27,28]. Finally, the samples were passivated at ambient temperature for 1 h under a flow (50 mL min⁻¹) of 5% O₂/N₂. The catalysts are denoted as ReC/support.

3.4. Catalyst Characterization

Textural properties were obtained by N₂ sorption isotherms at −196 °C using a 3-Flex device (Micromeritics, Norcross, GA, USA). Prior to the measurements, the samples were degassed at 300 °C for 4 h on a SmartVacPrep equipment (Micromeritics, Norcross, GA, USA). Surface area was obtained from the BET method and pore size distribution was obtained by the BJH model on the desorption branch of the N₂ isotherm. The total pore volume (v_T) was obtained from the quantity of N₂ adsorbed at $p/p^0 = 0.997$ and the micropore volume (V_μ) was determined from the t-plot equation. The mesopore volume (V_{meso}) was obtained from the difference between V_T and V_μ .

X-ray diffraction (XRD) measurements were carried out with a Polycrystal X'Pert ProPANalytical instrument (UK) using Ni-filtered Cu K α radiation $\lambda = 0.15406 \text{ nm}$ and a graphite monochromator. For each sample, Bragg's angles between 4° and 100° were scanned using a step size of 0.04° and a scanning rate of five steps per second.

X-ray photoelectron spectroscopy (XPS) measurements were carried out using an Escalab 200 R spectrometer (Thermo Fisher Scientific, Waltham, MA, USA) equipped with a hemispherical analyzer and a non-monochromatic Mg K X-ray radiation ($h\nu = 1253.6 \text{ eV}$) source. The binding energy (BE) was measured by reference to the C 1s peak at 284.6 eV, with an equipment error of less than 0.01 eV in the energy determinations. The spectra of Re 4f and C 1s were fitted to a combination of Gaussian–Lorentzian curves of variable proportions using the least-square regression. The following constraints were considered for Re 4f fitting: spin-orbit splitting of 2.43 eV, equal FWHM for the 4f 7/2 and 5/2, and a fixed area ratio of 4:3 for those two components.

The same 3Flex device (Micromeritics) was employed for CO chemisorption and temperature programmed reduction/desorption measurements. For the CO chemisorption, the samples were degassed in situ at 110 °C for 30 min and re-reduced at 350 °C for 30 min under H₂ flow (60 mL min⁻¹). CO chemisorption was carried out at 35 °C and the uptake was determined by subtracting two isotherms recorded consecutively with an evacuation step of 1 h between the two measurements.

Temperature-programmed reduction (TPR), temperature-programmed desorption of NH₃ (TPD-NH₃) and temperature-programmed decomposition of isopropylamine (TPD-IPA) were carried out with a combination of a thermal conductivity detector (TCD) and a mass spectrometer (Cirrus 2, MKS Instruments Inc., Andover, MA, USA). For the TPR measurement, the samples were heated at 10 °C min⁻¹ under 5% H₂/Ar flow

(100 mL min⁻¹). A cold trap was placed between the outlet of the reactor and the TCD to remove the water produced during reduction. The effluent stream was monitored by MS and the masses 15 (CH₄), 18 (H₂O), 28 (CO), and 44 (CO₂) were recorded. For the TPD-NH₃ measurement, the samples were pretreated under He (100 mL min⁻¹) at 500 °C for 30 min. The sample was then exposed to NH₃ (30 mL.min⁻¹) at 100 °C for 15 min, purged under He (100 mL min⁻¹) to remove physisorbed NH₃, and then heated under He at a rate of 10 °C min⁻¹ while monitoring the *m/z* = 17 (NH₃) signal. For the TPD-IPA measurement, the samples were pretreated under He (100 mL min⁻¹) at 500 °C for 30 min, subjected to pulses of IPA at 200 °C, and then heated under He at a rate of 10 °C min⁻¹ while monitoring the *m/z* = 17 (NH₃), 41 (propylene) and 44 (IPA) signals.

3.5. Catalytic Properties

Guaiacol conversion was carried out in a 100 mL stirred-batch reactor from Parr instrument. The catalyst (0.2 g) was introduced with guaiacol (1.7 g), dodecane (32 g) as the solvent, and hexadecane (700 µL) as the internal standard. The reactor was first purged for 10 min with N₂ flow and then heated to 350 °C under autogenous pressure and continuous stirring (645 rpm). An aliquot was first collected, and then hydrogen was introduced to the system to increase the total pressure to 5.0 MPa. Liquid samples were collected periodically during the course of the reaction (4 h) and were analyzed and quantified using a Nexis GC-2030 gas chromatograph (Shimadzu, Kyoto, Japan) equipped with an Elite-1 column (Perkin Elmer, Waltham, MA, USA, 30 m × 0.32 mm, film thickness of 0.25 µm) and an FID detector. The conversion was calculated by two equations (Equations (1) and (2)). The first equation is related to guaiacol disappearance, while the second equation is based on product formation. This allowed the carbon balance to be calculated (conversion from Equation (2) conversion from Equation (1)). Product selectivity was calculated by Equation (3), and the initial rate and conversion was obtained by Equation (4). Finally, turnover frequency (TOF) was defined according the sites probe by CO chemisorption (Equation (5)).

$$\text{Conversion (\%)} = \frac{n_{\text{GUA}}^0 - n_{\text{GUA}}}{n_{\text{GUA}}^0} \times 100 \quad (1)$$

$$\text{Conversion (\%)} = \frac{n_{\text{products}}}{n_{\text{reagent remaining}} + n_{\text{products}}} \times 100 \quad (2)$$

$$\text{Selectivity (\%)} = \frac{n_{\text{product } i}}{\sum n_{\text{products}}} \times 100 \quad (3)$$

$$r_0 = \frac{b \times n_{\text{GUA}}^0}{m} \quad (4)$$

$$\text{TOF} = \frac{r_0}{\text{CO uptake}} \quad (5)$$

In these equations, n_{GUA}^0 corresponds to the initial quantity (mol) of guaiacol, n_{GUA} is the quantity at a time *t*, n_{products} is the sum of all of the products detected (mol), $n_{\text{product } i}$ is the amount (mol) of a product *i*, *m* is the weight (g) of the catalyst, and *b* corresponds to the initial slope obtained by plotting conversion vs. time (s). In addition, $n_{\text{reagent remaining}}$ represents the difference between the quantity (mol) of guaiacol at the beginning of the reaction (n_{GUA}^0) and at a time *t*. For the calculation of the initial rates (Equation (4)), only the data at the low conversion region ($\leq 30\%$) were considered.

4. Conclusions

The present work provided strong evidence that the choice of support affects the carburization process. Over an inert support such as SiO₂, rhenium was not carburized but instead graphitic carbon was formed and Re⁰ was the main species detected at the surface. By using acidic supports carburization of rhenium occurred and depending on the surface and chemical identity of the support, different carbidic species were obtained. Over

ZrO₂, Re_xC was formed, whereas over Al₂O₃, Re₂C was obtained together with oxycarbide species. The most active catalyst was ReC/ZrO₂, followed by ReC/Al₂O₃, and then ReC/SiO₂, which was associated to co-participation of sites on the supports. In addition, clear differences in product selectivities were observed over the catalysts, consistent with the existence of different Re species and the possible involvement of the support in dictating the reaction routes. The ReC/SiO₂ was most selective to catechol, the ReC/ZrO₂ was active for direct formation of phenol, bypassing catechol, and the ReC/Al₂O₃ was most selective to phenol but also produced catechol. The desirable properties of ReC/ZrO₂ were attributed to the existence of Re_xC species and Brønsted acid sites on ZrO₂. Additionally, all of the catalysts produced an appreciable amount of desirable aromatic hydrocarbons (benzene and toluene), while minimizing excessive hydrogenation of the aromatic ring, an important distinction from previously reported results on activated carbon-supported Re carbides.

Author Contributions: Conceptualization, E.B.; methodology, E.B.; validation, E.B., I.T.G., A.B.D. and N.E.; formal analysis, E.B.; investigation, E.B., I.T.G., A.B.D. and N.E.; resources, I.T.G., A.B.D. and N.E.; writing—original draft preparation, E.B.; writing—review and editing, E.B., I.T.G., A.B.D. and N.E.; supervision, N.E.; project administration, E.B.; funding acquisition, E.B. and N.E. All authors have read and agreed to the published version of the manuscript.

Funding: This research was funded by Agencia Nacional de Investigación y Desarrollo (ANID) Chile, grants number Fondecyt N° 3170072, N° 1220763, Fondecup N° EQM160070, the Millennium Science Initiative Program—NCN2021_090 and European Union 101008058.

Data Availability Statement: Not applicable.

Conflicts of Interest: The authors declare no conflict of interest.

References

1. Zakzeski, J.; Weckhuysen, B.M. Lignin Solubilization and Aqueous Phase Reforming for the Production of Aromatic Chemicals and Hydrogen. *ChemSusChem* **2011**, *4*, 369–378. [[CrossRef](#)] [[PubMed](#)]
2. French, R.J.; Stunkel, J.; Baldwin, R.M. Mild Hydrotreating of Bio-Oil: Effect of Reaction Severity and Fate of Oxygenated Species. *Energy Fuels* **2011**, *25*, 3266–3274. [[CrossRef](#)]
3. Zakzeski, J.; Bruijninx, P.C.A.; Jongerijs, A.L.; Weckhuysen, B.M. The Catalytic Valorization of Lignin for the Production of Renewable Chemicals. *Chem. Rev.* **2010**, *110*, 3552–3599. [[CrossRef](#)] [[PubMed](#)]
4. Saidi, M.; Samimi, F.; Karimipourfard, D.; Nimmanwudipong, T.; Gates, B.C.; Rahimpour, M.R. Upgrading of lignin-derived bio-oils by catalytic hydrodeoxygenation. *Energy Environ. Sci.* **2014**, *7*, 103–129. [[CrossRef](#)]
5. Bui, V.N.; Laurenti, D.; Afanasiev, P.; Geantet, C. Hydrodeoxygenation of guaiacol with CoMo catalysts. Part I: Promoting effect of cobalt on HDO selectivity and activity. *Appl. Catal. B* **2011**, *101*, 239–245. [[CrossRef](#)]
6. Chang, J.; Danuthai, T.; Dewiyanti, S.; Wang, C.; Borgna, A. Hydrodeoxygenation of Guaiacol over Carbon-Supported Metal Catalysts. *ChemCatChem* **2013**, *5*, 3041–3049. [[CrossRef](#)]
7. Bomont, L.; Alda-Onggar, M.; Fedorov, V.; Aho, A.; Peltonen, J.; Eränen, K.; Peurla, M.; Kumar, N.; Wärnå, J.; Russo, V.; et al. Production of Cycloalkanes in Hydrodeoxygenation of Isoeugenol Over Pt- and Ir-Modified Bifunctional Catalysts. *Eur. J. Inorg. Chem.* **2018**, *2018*, 2841–2854. [[CrossRef](#)]
8. Blanco, E.; Dongil, A.B.; Escalona, N. Synergy between Ni and Co Nanoparticles Supported on Carbon in Guaiacol Conversion. *Nanomaterials* **2020**, *10*, 2199. [[CrossRef](#)]
9. Huynh, T.M.; Armbruster, U.; Pohl, M.-M.; Schneider, M.; Radnik, J.; Hoang, D.-L.; Phan, B.M.Q.; Nguyen, D.A.; Martin, A. Hydrodeoxygenation of Phenol as a Model Compound for Bio-oil on Non-noble Bimetallic Nickel-based Catalysts. *ChemCatChem* **2014**, *6*, 1940–1951. [[CrossRef](#)]
10. Jiang, L.; Zhou, P.; Liao, C.; Zhang, Z.; Jin, S. Cobalt Nanoparticles Supported on Nitrogen-Doped Carbon: An Effective Non-Noble Metal Catalyst for the Upgrade of Biofuels. *ChemSusChem* **2018**, *11*, 959–964. [[CrossRef](#)]
11. Ghampson, I.T.; Sepulveda, C.; Garcia, R.; Fierro, J.L.G.; Escalona, N. Carbon nanofiber-supported ReOx catalysts for the hydrodeoxygenation of lignin-derived compounds. *Catal. Sci. Technol.* **2016**, *6*, 4356–4369. [[CrossRef](#)]
12. Lødeng, R.; Ranga, C.; Rajkhowa, T.; Alexiadis, V.I.; Björkan, H.; Chytil, S.; Svenum, I.H.; Walmsley, J.; Thybaut, J.W. Hydrodeoxygenation of phenolics in liquid phase over supported MoO₃ and carburized analogues. *Biomass Convers. Biorefinery* **2017**, *7*, 343–359. [[CrossRef](#)]
13. Shetty, M.; Murugappan, K.; Prasomsri, T.; Green, W.H.; Román-Leshkov, Y. Reactivity and stability investigation of supported molybdenum oxide catalysts for the hydrodeoxygenation (HDO) of m-cresol. *J. Catal.* **2015**, *331*, 86–97. [[CrossRef](#)]
14. Ghampson, I.T.; Sepulveda, C.; Garcia, R.; Frederick, B.G.; Wheeler, M.C.; Escalona, N.; DeSisto, W.J. Guaiacol transformation over unsupported molybdenum-based nitride catalysts. *Appl. Catal. A* **2012**, *413–414*, 78–84. [[CrossRef](#)]

15. Sepúlveda, C.; Leiva, K.; García, R.; Radovic, L.R.; Ghampson, I.T.; DeSisto, W.J.; Fierro, J.L.G.; Escalona, N. Hydrodeoxygenation of 2-methoxyphenol over Mo₂N catalysts supported on activated carbons. *Catal. Today* **2011**, *172*, 232–239. [[CrossRef](#)]
16. Akhmetzyanova, U.; Tišler, Z.; Sharkov, N.; Skuhrovcová, L.; Pelišková, L.; Kikhtyanin, O.; Mäki-Arvela, P.; Opanasenko, M.; Peurla, M.; Murzin, D.Y. Molybdenum Nitrides, Carbides and Phosphides as Highly Efficient Catalysts for the (hydro)Deoxygenation Reaction. *ChemistrySelect* **2019**, *4*, 8453–8459. [[CrossRef](#)]
17. Feitosa, L.F.; Berhault, G.; Laurenti, D.; Teixeira da Silva, V. Effect of the Nature of the Carbon Support on the Guaiacol Hydrodeoxygenation Performance of Nickel Phosphide: Comparison between Carbon Nanotubes and a Mesoporous Carbon Support. *Ind. Eng. Chem. Res.* **2019**, *58*, 16164–16181. [[CrossRef](#)]
18. Ted Oyama, S.; Onkawa, T.; Takagaki, A.; Kikuchi, R.; Hosokai, S.; Suzuki, Y.; Bando, K.K. Production of Phenol and Cresol from Guaiacol on Nickel Phosphide Catalysts Supported on Acidic Supports. *Top. Catal.* **2015**, *58*, 201–210. [[CrossRef](#)]
19. Jongerius, A.L.; Gosselink, R.W.; Dijkstra, J.; Bitter, J.H.; Bruijninx, P.C.A.; Weckhuysen, B.M. Carbon Nanofiber Supported Transition-Metal Carbide Catalysts for the Hydrodeoxygenation of Guaiacol. *ChemCatChem* **2013**, *5*, 2964–2972. [[CrossRef](#)]
20. Ochoa, E.; Torres, D.; Moreira, R.; Pinilla, J.L.; Suelves, I. Carbon nanofiber supported Mo₂C catalysts for hydrodeoxygenation of guaiacol: The importance of the carburization process. *Appl. Catal. B* **2018**, *239*, 463–474. [[CrossRef](#)]
21. Santillan-Jimenez, E.; Perdu, M.; Pace, R.; Morgan, T.; Crocker, M. Activated Carbon, Carbon Nanofiber and Carbon Nanotube Supported Molybdenum Carbide Catalysts for the Hydrodeoxygenation of Guaiacol. *Catalysts* **2015**, *5*, 424–441. [[CrossRef](#)]
22. Pang, J.; Sun, J.; Zheng, M.; Li, H.; Wang, Y.; Zhang, T. Transition metal carbide catalysts for biomass conversion: A review. *Appl. Catal. B* **2019**, *254*, 510–522. [[CrossRef](#)]
23. Führer, M.; van Haasterecht, T.; Bitter, J.H. Molybdenum and tungsten carbides can shine too. *Catal. Sci. Technol.* **2020**, *10*, 6089–6097. [[CrossRef](#)]
24. Smith, K.J. Metal carbides, phosphides, and nitrides for biomass conversion. *Curr. Opin. Green Sustain. Chem.* **2020**, *22*, 47–53. [[CrossRef](#)]
25. Mortensen, P.M.; de Carvalho, H.W.P.; Grunwaldt, J.-D.; Jensen, P.A.; Jensen, A.D. Activity and stability of Mo₂C/ZrO₂ as catalyst for hydrodeoxygenation of mixtures of phenol and 1-octanol. *J. Catal.* **2015**, *328*, 208–215. [[CrossRef](#)]
26. Blanco, E.; Sepulveda, C.; Cruces, K.; García-Fierro, J.L.; Ghampson, I.T.; Escalona, N. Conversion of guaiacol over metal carbides supported on activated carbon catalysts. *Catal. Today* **2020**, *356*, 376–383. [[CrossRef](#)]
27. Blanco, E.; Dongil, A.B.; García-Fierro, J.L.; Escalona, N. Insights in supported rhenium carbide catalysts for hydroconversion of lignin-derived compounds. *Appl. Catal. A* **2020**, *599*, 117600. [[CrossRef](#)]
28. Blanco, E.; Dongil, A.B.; Ghampson, I.T.; García-Fierro, J.L.; Escalona, N. Optimizing the carburization conditions of supported rhenium carbide for guaiacol conversion. *Appl. Catal. A* **2021**, *623*, 118267. [[CrossRef](#)]
29. Bui, V.N.; Laurenti, D.; Delichère, P.; Geantet, C. Hydrodeoxygenation of guaiacol: Part II: Support effect for CoMoS catalysts on HDO activity and selectivity. *Appl. Catal. B* **2011**, *101*, 246–255. [[CrossRef](#)]
30. De Souza, P.M.; Rabelo-Neto, R.C.; Borges, L.E.P.; Jacobs, G.; Davis, B.H.; Sooknoi, T.; Resasco, D.E.; Noronha, F.B. Role of Keto Intermediates in the Hydrodeoxygenation of Phenol over Pd on Oxophilic Supports. *ACS Catal.* **2015**, *5*, 1318–1329. [[CrossRef](#)]
31. Lin, S.S.Y.; Thomson, W.J.; Hagensen, T.J.; Ha, S.Y. Steam reforming of methanol using supported Mo₂C catalysts. *Appl. Catal. A* **2007**, *318*, 121–127. [[CrossRef](#)]
32. Brungs, A.J.; York, A.P.E.; Claridge, J.B.; Marquez-Alvarez, C.; Green, M.L.H. Dry reforming of methane to synthesis gas over supported molybdenum carbide catalysts. *Catal. Lett.* **2000**, *70*, 117–122. [[CrossRef](#)]
33. Leiva, K.; Martinez, N.; Sepulveda, C.; García, R.; Jiménez, C.A.; Laurenti, D.; Vrinat, M.; Geantet, C.; Fierro, J.L.G.; Ghampson, I.T.; et al. Hydrodeoxygenation of 2-methoxyphenol over different Re active phases supported on SiO₂ catalysts. *Appl. Catal. A* **2015**, *490*, 71–79. [[CrossRef](#)]
34. Greiner, M.T.; Rocha, T.C.R.; Johnson, B.; Klyushin, A.; Knop-Gericke, A.; Schlögl, R. The Oxidation of Rhenium and Identification of Rhenium Oxides During Catalytic Partial Oxidation of Ethylene: An In-Situ XPS Study. *Z. Phys. Chem.* **2014**, *228*, 521–541. [[CrossRef](#)]
35. Abou Hamdan, M.; Loridant, S.; Jahjah, M.; Pinel, C.; Perret, N. TiO₂-supported molybdenum carbide: An active catalyst for the aqueous phase hydrogenation of succinic acid. *Appl. Catal. A* **2019**, *571*, 71–81. [[CrossRef](#)]
36. Chen, X.; Wang, X.; Fang, D. A review on C1s XPS-spectra for some kinds of carbon materials. *Fuller. Nanotub. Carbon Nanostructures* **2020**, *28*, 1048–1058. [[CrossRef](#)]
37. Leiva, K.; Garcia, R.; Sepulveda, C.; Laurenti, D.; Geantet, C.; Vrinat, M.; Garcia-Fierro, J.L.; Escalona, N. Conversion of guaiacol over supported ReOx catalysts: Support and metal loading effect. *Catal. Today* **2017**, *296*, 228–238. [[CrossRef](#)]
38. Lee, J.S.; Oyama, S.T.; Boudart, M. Molybdenum carbide catalysts: I. Synthesis of unsupported powders. *J. Catal.* **1987**, *106*, 125–133. [[CrossRef](#)]
39. Miyao, T.; Shishikura, I.; Matsuoka, M.; Nagai, M.; Oyama, S.T. Preparation and characterization of alumina-supported molybdenum carbide. *Appl. Catal. A* **1997**, *165*, 419–428. [[CrossRef](#)]
40. Figueiredo, J.L.; Pereira, M.F.R.; Freitas, M.M.A.; Órfão, J.J.M. Modification of the surface chemistry of activated carbons. *Carbon* **1999**, *37*, 1379–1389. [[CrossRef](#)]
41. Blanco, E.; Díaz de León, J.N.; García-Fierro, J.L.; Escalona, N. Study of supported bimetallic MoRe carbides catalysts for guaiacol conversion. *Catal. Today* **2021**, *367*, 290–296. [[CrossRef](#)]

42. Pereira, C.; Gorte, R.J. Method for distinguishing Brønsted-acid sites in mixtures of H-ZSM-5, H-Y and silica-alumina. *Appl. Catal. A* **1992**, *90*, 145–157. [[CrossRef](#)]
43. Iglesia, E.; Ribeiro, F.H.; Boudart, M.; Baumgartner, J.E. Synthesis, characterization, and catalytic properties of clean and oxygen-modified tungsten carbides. *Catal. Today* **1992**, *15*, 307–337. [[CrossRef](#)]
44. Iglesia, E.; Baumgartner, J.E.; Ribeiro, F.H.; Boudart, M. Bifunctional reactions of alkanes on tungsten carbides modified by chemisorbed oxygen. *J. Catal.* **1991**, *131*, 523–544. [[CrossRef](#)]
45. Iglesia, E.; Ribeiro, F.H.; Boudart, M.; Baumgartner, J.E. Tungsten carbides modified by chemisorbed oxygen. A new class of bifunctional catalysts. *Catal. Today* **1992**, *15*, 455–458. [[CrossRef](#)]
46. He, Y.; Bie, Y.; Lehtonen, J.; Liu, R.; Cai, J. Hydrodeoxygenation of guaiacol as a model compound of lignin-derived pyrolysis bio-oil over zirconia-supported Rh catalyst: Process optimization and reaction kinetics. *Fuel* **2019**, *239*, 1015–1027. [[CrossRef](#)]
47. Mora, I.D.; Méndez, E.; Duarte, L.J.; Giraldo, S.A. Effect of support modifications for CoMo/ γ -Al₂O₃ and CoMo/ASA catalysts in the hydrodeoxygenation of guaiacol. *Appl. Catal. A* **2014**, *474*, 59–68. [[CrossRef](#)]
48. Silva, N.K.G.; Ferreira, R.A.R.; Ribas, R.M.; Monteiro, R.S.; Barrozo, M.A.S.; Soares, R.R. Gas-phase hydrodeoxygenation (HDO) of guaiacol over Pt/Al₂O₃ catalyst promoted by Nb₂O₅. *Fuel* **2021**, *287*, 119509. [[CrossRef](#)]
49. Martínez, N.; García, R.; Fierro, J.L.G.; Wheeler, C.; Austin, R.N.; Gallagher, J.R.; Miller, J.T.; Krause, T.R.; Escalona, N.; Sepúlveda, C. Effect of Cu addition as a promoter on Re/SiO₂ catalysts in the hydrodeoxygenation of 2-methoxyphenol as a model bio oil compound. *Fuel* **2016**, *186*, 112–121. [[CrossRef](#)]
50. Znaiguia, R.; Brandhorst, L.; Christin, N.; Bellière Baca, V.; Rey, P.; Millet, J.-M.M.; Loridant, S. Toward longer life catalysts for dehydration of glycerol to acrolein. *Microporous Mesoporous Mater.* **2014**, *196*, 97–103. [[CrossRef](#)]